ISSN1027-5495. Functional Materials, 31, No.4 (2024), p. 520-526
doi:http://dx.doi.org/10.15407/fm31.04.520

Influence of hydrogenation on the structural state and properties of Zr1Nb alloy

V.I. Sokolenko, D.G. Malykhin, V.S. Okovit, R.V. Azhazha, A.O. Chupikov, P.O. Kutsenko, O.P. Ledeniov, O.Yu. Roskoshna, O.A Datsenko

National Science Center "Kharkiv Institute of Physics and Technology", Kharkiv, Ukraine,

Received July 2, 2024

It has been shown that during electrolytic hydrogenation of wire samples of the Zr1Nb alloy, a layer of 9.5 μm thick anisotropic zirconium hydride nanocrystals with a thickness of ≈9.5 μm is formed on the surface, which leads to a decrease in the shear modulus by 10% in pre-annealed samples and to a significantly reduced effect in deformed ones. The latter is a consequence of the competition of two factors: a decrease in modulus due to the direct formation of the δ hydride $ZrH_{1.66}$ and an increase due to the relaxation of internal stresses. The observed effect of a decrease in the electrical resistivity of a wire sample as a result of hydrogenation is discussed.

Keywords: Zr1Nb alloy, hydrogenation, structural state, properties

Вплив гідрівання на структурний стан і властивості сплаву Zr1Nb. *В.І. Соколенко, Д.Г. Малихін, В.С. Оковіт, Р.В. Ажажа, А.О. Чупіков, П.О. Куценко, О.П.Леденьов, О.Ю. Роскошна, О.А.Даценко*

Показано, що при електролітичному гідруванні дротяних зразків сплаву Zr1Nb відбуваються утворення на поверхні шару товщиною анізотропних нанокристалів δ гідриду цирконію товщиною ≈9,5 мкм, що призводить до зменшення модулю зсуву на 10% у попередньо відпалених зразках і значно слабшого ефекту у деформованих. Останнє є наслідком конкуренції двох факторів: зменшення модуля за рахунок безпосереднього утворення δ гідриду $ZrH_{1.66}$ та збільшення за рахунок релаксації внутрішніх напружень. Обговорюються спостережуваний ефект зменшення питомого електроопору дротяного зразка внаслідок гідрування.

1. Introduction

Zirconium alloys, due to a unique combination of properties, namely a small thermal neutron scattering cross section, high corrosion resistance, acceptable mechanical properties and manufacturability, are the main structural material for existing and prospective thermal nuclear reactors. During the operation of zirconium materials, their tendency to absorb hydrogen is revealed, which is formed due to both radiolysis of the coolant [1] and nuclear hydrogenation of fuel element shell [2]. The main manifestations of the degradation of zirconium materials with the participation of hydrogen include embrittlement (a sharp decrease in plasticity during hydrogenation), the formation of large massive hydrides (defects of the "solar corona" type, blisters) and delayed hydride cracking [3-6].

When studying the processes and mechanisms of hydrogenation of α-Zr as the basic element of zirconium alloys, two methods are used to create zirconium hydrides of different stoichiometric composition, namely: 1) through the penetration of hydrogen into the crystal lattice due to its release and absorption in electrochemical corrosion processes; 2) during thermal diffusion into the crystal lattice. The second method pro-

motes an enhanced hydrogenation process at a temperature of 700°C and Fe above. It is clear that at such temperatures the initial structural state of zirconium materials changes, which may affect the hydrogenation process and the nature of the change in properties as a result of hydrogenation. During normal operation of nuclear reactors of the VVER-1000 type, the temperature of the fuel cell shell in the coolant surface boiling mode is ~350°C, which has a relatively weak influence on the change in the structural state. Thus, when studying changes in the structural-phase composition and properties of zirconium materials using electrolytic saturation, which is carried out at temperatures close to room temperature, the effects of hydrogenation will correspond to the previously formed structural state.

As for the electrolytic hydrogenation of zirconium, in [7] the processes of near-surface hydride aging, as well as the mechanisms underlying the release of hydrides and their distribution in the microstructure of pure Zr, were studied in detail using the methods of X-ray diffraction (XRD), scanning electron microscopy (SEM, SU6600), transmission electron microscopy (TEM, JEOL 2100F). It is known that the Zr1Nb alloy is characterized by a very low concentration of niobium in the solid solution; therefore, the resulting hydrogenation effects will be mainly related to the zirconium matrix. The aim of our work was to obtain data on the relationship between changes in the structural-phase composition and mechanical (shear modulus) and electrophysical (electrical resistance) properties of Zr1Nb alloy samples during electrolytic hydrogenation.

2. Experimental

The alloy Zr-1wt.% Nb (accepted designation Zr1Nb) was made on the basis of calcium-thermal zirconium [8]; the impurity content is given in Table 1. Wire samples in two structural states, namely TMT–1 and TMT–2, were studied. The structural state of TMT–1 was formed as a result of a sequence of several stages of thermomechanical processing. A bar with a diameter of 10 mm was deformed by drawing at 400°C to a diameter of 1.5 mm and further at 300°C to a final diameter of 0.8 mm; the wire was then annealed in vacuum at 65Fe0°C for 1 hour. The second sample, TMT–2, differed in its structural state in that the drawing from a diameter of 4.5 mm was carried out at room temperature to a final diameter of 0.8 mm without annealing of the wire. In the TMT–1 and TMT–2 samples, the hydrogen content in the initial state did not exceed 16 ppm.

Samples of 45 mm length were hydrogenated in an electrochemical cell with a platinum anode. The electrolyte was a one-normal solution of sulfuric acid with the addition of 1.5 g/l of thiourea. The depth of immersion of the samples in the electrolyte was 5 cm. The cathode current density was 1.25 A/cm^2. Hydrogenation was carried out for 5 and 7 hours at an electrolyte temperature of 60°C. The U8 circulating liquid thermostat ensured a deviation of the electrolyte temperature within ± 0.1°C from the set value. The X-ray method was used to analyze the structural-phase state of the near-surface layers of hydrogenated samples. A standard 4-point potentiometric scheme allowed measuring the electrical resistance of the samples at 300 and 77 K. The reverse torsional pendulum technique was used to measure the shear modulus.

3. Results and discussion

Shear modulus. Shear modulus G for TMT–1 and TMT–2 samples was calculated according to the formula [9]: $G = A \times l \times f^2/d^4$, where A=const, l is the length of the working part and d is the diameter of the wire sample, f is the natural frequency of torsional oscillations. With known measurement errors of the values

Table 1. The amount of impurities in the ingot of the Zr1Nb alloy, wt.% [8].

O	N	C	Hf	F	Nb	Si	Fe
0,07-0,93	$(8\text{-}14)\cdot10^{-4}$	$(8\text{-}10)\cdot10^{-3}$	$(15\text{-}36)\cdot10^{-3}$	$<5\cdot10^{-4}$	0.94-1.02	$(1\text{-}2)\cdot10^{-3}$	$12\cdot10^{-3}$
Ni	Al O	Cu	Ca	Mn	Ti	Cr	Mo
$(2\text{-}3)\cdot10^{-3}$	$(11\text{-}22)\cdot10^{-5}$	$(24\text{-}45)\cdot10^{-4}$	$<5\cdot10^{-4}$	$<5\cdot10^{-4}$	$<10^{-4}$	$(10\text{-}16)\cdot10^{-4}$	$<10^{-3}$
Cd	K	Li	Cl	Pb	B	Be	
$<10^{-5}$	$<5\cdot10^{-4}$	$<10^{-5}$	$5\cdot10^{-4}$	$<10^{-3}$	$<5\cdot10^{-4}$	$<5\cdot10^{-4}$	

Table 2 – Shear moduli G_i and average values of $\langle G \rangle$

Hydrogenation time t, hrs.	Shear modulus			
	TMT–1		TMT–2	
	G, MPa			
	G_i	$\langle G \rangle$	G_i	$\langle G \rangle$
-	34720	34475	31720	32065
			32010	
	34230		32510	
			32010	
5	33270	33520	-	
	33560			
7	30460	30510	32330	32685
			32770	
	30660		32750	
			32890	

in the given formula (Δl=0.1 mm, Δd=0.005 mm, $\Delta f/f<5 \cdot 10^{-4}$), the shear modulus measurement error is 0.3%.

Table 2 presents the shear modulus G_i data for individual samples and the average values of $\langle G \rangle$ at room temperature. The table shows that when measuring a batch of samples in the same structural state, the spread of G values does not exceed 1.3%. To analyze the obtained data, it is convenient to use the average values of the shear modulus. A comparison of the characteristics of the annealed (TMT–1) and deformed (TMT–2) samples shows that the deformation leads to a decrease in the modulus due to the presence of deformation defects (dislocations and point defects). Such defects lead to local breaks in electron bonds and a decrease in the degree of overlap of electron wave functions of neighboring atoms, which is reflected in a decrease in the shear modulus. In addition, the reduced modulus of deformed samples will be due to the viscoelastic effect of dislocation mobility (Frank-Reed loops) and, perhaps even to a greater extent, the mobility of twin boundaries of deformation origin [10].

As can be seen from Table 2, hydrogenation has different effects on the shear modulus of TMT–1 and TMT–2 samples. For the material in the annealed state (TMT–1), hydrogenation leads to a decrease in the average value of the shear modulus: by ≈3% after exposure t = 5 h and by ≈10% after t=7 h. The material in the deformed state (TMT–2) is characterized by a slight increase in $\langle G \rangle$ due to hydrogenation (t=7 h). When determining G by the reversible torsion pendulum method, the data mainly refer to the metal layer near the surface of the cylindrical sample. Therefore, it was necessary to carry out X-ray studies of the samples in order to find out the nature of changes in the structural and phase composition due to hydrogenation, which affects the change in the shear modulus.

Structural and phase composition. The structural state and phase composition of the materials were analyzed by XRD method. X-ray diffraction patterns of a set of wire samples were recorded on a DRON4-07 diffractometer in a Bragg-Brentano X-ray optical scheme with a pair of Soller slits in CuK_α radiation and with digital data recording.

Fig.1 shows full-profile X-ray diffraction patterns from wire samples in the annealed state before and after hydrogenation. The measurements were carried out normal to the surface of the set of wire samples. Fig.1a is a typical spectrum of α-Zr with a textural maximum (002) in the selected direction. At angles of 38.5° and 55.6°, there are weak reflections from the β–Nb phase with a lattice period of 0.330 nm characteristic of pure niobium. At the same time, the X-ray pattern of the matrix according to the lattice periods (a=0.323 nm, c=0.515 nm) exactly corresponds to pure zirconium.

In Fig. 1b, reflections from the initial composition of the samples are practically absent. The available reflections belong to δ-hydride with an fcc lattice and a period of 0.4785...0.4790 nm, which is close to literature data (Table 3). At the same time, its texture is manifested with a maximum in the (111) reflection.

The thickness of the near-surface layer of δ-hydride was estimated from the traces of reflection from α-Zr on the X-ray pattern of hydrogenated TMT-1 samples. Data on the absorption coefficient of Cu-K_α radiation by zir-

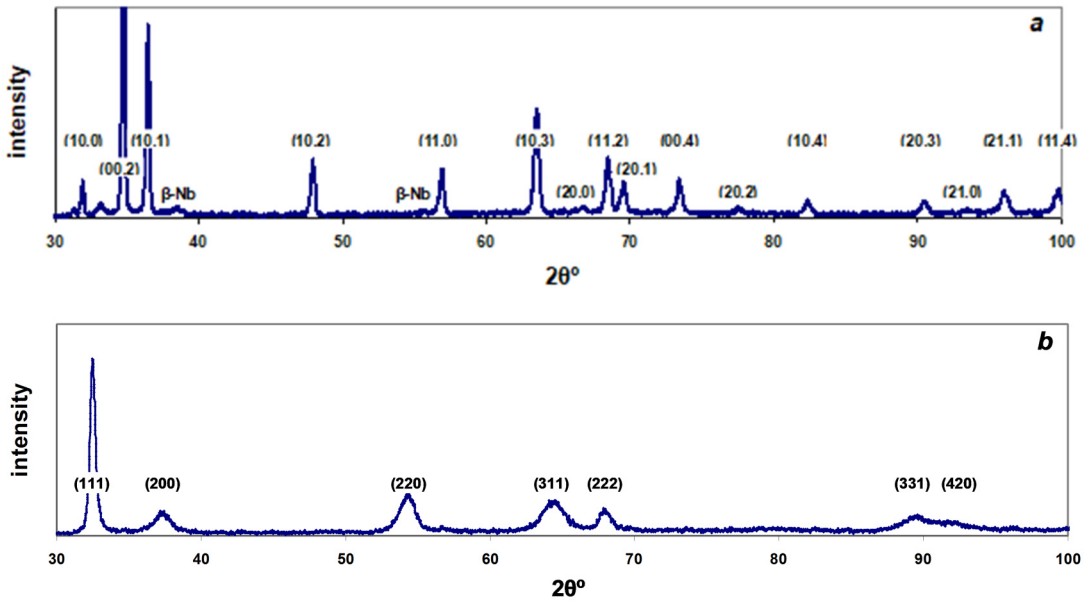

Fig. 1. X-ray diffraction patterns in Cu-K_α for samples of annealed Zr1Nb wire (TMT-1): before hydrogenation (a); after hydrogenation (b).

Table 3. Characteristics of crystal structure of Zr hydrides [12].

Phase	Formula	Crystal structure	Lattice parameters, nm
δ-hydride	$ZrH_{1.66}$	fcc	a = 0.4781
ε-hydride	ZrH_2	fct	a = 0.3520 c = 0.4450
γ-hydride	ZrH	fct	a = 0.4596 c = 0.4969

conium were used in the calculations [11]. The calculated value of the average thickness of the hydride layer was ≈9.5 μm. The analysis of the diffraction line widths (Fig. 2b) established that the hydride layer consists of crystalline fragments with a large difference in size (*d*); sharp differences are observed between crystallites with (111) and (200) orientations along the normal to the wire surface. Consequently, $d_{(111)} >$ 100 nm, $d_{(200)} \sim 6$ nm.

This result is explained by the following scenario of the process of hydrogen saturation of zirconium wire samples: hydride begins to form first of all in those fragments where hydrogen diffusion in depth is the lowest. The normal to the (0002) plane, corresponding to the texture maximum of reflection from the zirconium wire material, basically coincides with this diffusion direction. This plane is known to be a trigonal grid of zirconium atoms with a period of a_{Zr} = 0.323 nm. As mentioned above, the crystallographic plane (111) of the δ-hydride, formed as an immersion phase, basically coincides with its spatial orientation. This is also a trigonal grid with a trigonal period $a_{\delta\text{-H}}/\sqrt{2}$ =0.338 nm, according to the obtained results and data in Table 2, which differs by 4.5% from the size of the zirconium atomic network. In the absence of macrostresses in the annealed samples (TMT-1), the crystal plane (0002) of α-Zr can be considered the preferred habit plane for the formation of δ-hydride [13, 14].

Thus, the preferential crystallographic orientation of δ-hydride precipitates and their dimensional anisotropy in Zr1Nb wire samples can be associated with the crystallographic texture of the wire, which determines the least favorable direction for hydrogen diffusion.

According to the generally accepted point of view, tensile stresses in zirconium materials (in particular, in the Zircaloy-4 alloy), reaching a certain value, contribute to the allocation of planes of crystallographic habit that are different from the (0002) plane (see, e.g., [10]) and their actual reorientation as areas of hydride allocation. This, in turn, will give a noticeable effect when observing the relaxation of elastic stresses, in particular, when we use the torsional vibration method.

Modulus change due to hydrogenation. Let us consider the reasons for the decrease of the shear modulus as a result of hydrogenation of the annealed sample and the insignificant recovery of the modulus of the deformed sample.

In our analysis, only changes in the structural-phase state of the zirconium matrix, which makes up about 99% of the sample, will be taken into account, while the possible influence of hydrogenation of inclusions of the niobium ß-phase will be insignificant, given the influence of the mixture law in determining the shear modulus. Then there is every reason to believe that the annealed sample (TMT−1), consisting crystals with hcp lattice, is characterized by a minimum level of internal stresses. As a result of hydrogenation near the surface to a depth of ≈9.3 μm, a layer of anisotropic fcc nanocrystals of δ-phase (about 5% of the volume) with a lattice parameter a = 0.4781 nm is formed. In general, when using the inverse torsion pendulum method, the obtained data on the elastic modulus contain some averaged information about the fcc δ-phase and the hcp α-phase, as well as an invariable definite contribution due to inclusions of the ß-phase of niobium. Considering the fact that during the hydrogenation process the measured value of the modulus decreased by ≈3% after holding for t = 5 h and by ≈10% after t = 7 h, it can be concluded that the δ-phase of zirconium hydride has at least 10% lower shear modulus compared to the hcp α-phase of zirconium.

For the deformed sample (TMT–2) there is a decrease in modulus by ≈7% compared to the annealed sample (TMT–1). When hydrating TMT–2 samples, factors of internal stress and the presence of deformation defects clearly appear. In the process of hydrogenation, there will be a redistribution of dislocations in clusters as a result of the movement of interphase boundaries during the growth of δ-phase crystallites. In addition, there is a reorientation of the planes of the hydride precipitates, which were mentioned above. As a result, there is competition between two factors: a decrease in the modulus due to the immediate formation of the δ-phase and a recovery due to the relaxation of internal stresses. At the same time, the significance of these factors is largely comparable: the shear modulus before and after hydrogenation differs by 2% (see Table 2). It follows from the above that the change in the shear modulus characterizing the mechanical stability of materials, in the case of the formation of the hydride δ-phase largely depends on the structural state. In the annealed state, the formation of the hydride phase is accompanied by a significant (≈10%) decrease in the shear modulus. In the deformed material, the hydride phase is characterized by a very weak change in G. This behavior of the shear modulus manifests itself in the strength and ductility characteristics of hydrogenated zirconium materials.

Electrical resistivity change due to hydrogenation. Let us consider the possible reasons for the observed change in electrical resistivity ρ of Zr1Nb alloy samples in the annealed state (TMT-1) as a result of hydrogenation. In general, the influence of hydrogen on the electrophysical properties of metals is ambiguous. If for non-transition metals hydrogen dissolved in the lattice acts as a factor of additional scattering of carriers, then in the case of metals with unfilled d-shells the picture becomes more complicated. In [15] it was noted that as a result of hydrogenation a metal-hydrogen zone arises below the level of the d-zone of the metal; in this case, the s-d-electrons move into this new zone, and some of the states shift below the Fermi level and it shifts upward due to the difference in the number of electrons received from hydrogen and the number of new electron states. Such features of changes in the band structure during hydrogenation are confirmed, in particular, by the results of studies of the palladium–hydrogen system carried out by the APW method [16]. It is shown that metallic Pd and hydrides of the composition $PdH_{0.6}$ and PdH are characterized by Fermi energies of ≈0.51, ≈0.60 and ≈0.62 Ry, respectively. For the magnetically ordered metal Dy, similar changes in the energy spectrum as a result of solid solution hydrogenation cause a decrease in the values of the phase magnetic transition temperatures and the contribution to ρ(T) related to electron scattering in the paramagnetic phase with an increase in the residual electrical resistance [17]. At the same time, the DyH_2 phase is characterized by a higher conductivity compared to the non-hydrogenated material [18]. The above makes it possible to qualitatively analyze the effect of hydrogenation for the Zr1Nb alloy as applied to the zirconium matrix.

Table 4 presents the values of ρ_{300K} and ρ_{77K} for samples TMT–1 and TMT–2 in the initial state, as well as the characteristics of Zr samples (reactor grade) and some samples of ZrH_x hydrides (x=1.63...1.96) [19].

Table 4. Characteristics of Zr1Nb, Zr and Zr hydrides.

Samples	State	$\rho_{300\ K}$	$\rho_{77\ K}$	Crystal structure by X-rays	Ref.
		μΩ·cm			
Zr1Nb (TMT–1)	metallic annealed	48.9	12.0	hcp (Zr) + bcc (Nb)	presented work
	metallic + hydride	42.8	7.0	hcp (Zr)+fcc ($ZrH_{1.66}$)+bcc (Nb)	presented work
Zr (reactor grade)	metallic	50.8	12.2	hcp	[19]
$ZrH_{1.63}$	hydride	73.2	51.1	fcc	[19]
$ZrH_{1.74}$	hydride	60.2	38.7	fct	[19]
$ZrH_{1.81}$	hydride	54.7	33.2	fct	[19]
$ZrH_{1.96}$	hydride	24.7	7.82	fct	[19]

From Table 4 it can be seen that the TMT–1 (annealed) and Zr (reactor grade) samples are characterized by fairly close electrical resistivity values and the difference is due to the presence of fine inclusions of pure niobium in the zirconium matrix, which act as additional scattering centers for conduction electrons. The non-monotonic change in the specific electrical resistance of zirconium hydride samples compared to the characteristics of Zr (reactor grade) is noteworthy [18]. The values of ρ_{300K} and ρ_{77K} noticeably increase for the hydride $ZrH_{1.63}$ (fcc lattice), and then decrease for the hydrides $ZrH_{1.74}$ and $ZrH_{1.81}$, reaching minimum values for $ZrH_{1.96}$. The observed effect of reducing electrical resistivity is associated with the higher conductivity of fct crystal lattice of hydrides compared to the fcc lattice.

In the hydrogenated Zr1Nb wire sample, the hydrogen content varies unevenly along the radius. Let us consider at a qualitative level the factors that determine the value of the electrical resistance of such a sample. In its central part, hydrogen is present as an impurity implanted into the hcp lattice of the zirconium matrix, which manifests itself as additional charge carrier scattering centers. A near-surface layer of nanograins of δ-hydride $ZrH_{1.66}$, like the hydride $ZrH_{1.63}$ (Table 3), will also have a higher electrical resistance compared to the annealed state of Zr1Nb. The question arises about a possible factor in the reduction in electrical resistance, which was observed in the experiment.

Table 4 shows that ε-hydride with face-centered tetragonal lattice (fct, $a<c$) with a ratio of H/Zr=1.96 has an electrical resistivity at 300 K that is 40% less than for pure Zr, and at T = 77, the values of the electrical resistivity are close. It can be assumed that a very thin layer of ε-hydride is created near the surface of the hydrated sample, which shunts deeper growing balls with higher values of electrical resistivity. The amount of this hydride is too small to be identified by conventional techniques for the analysis of large-volume samples. In work [7], complex structural studies of electrolytically hydrogenated thin high-purity Zr foils with an average grain size of ~85 μm revealed reflections of the fct ε-phase $ZrH_{1.801}$. These very weak reflections appeared after hydration for t=48 h at a current density of 0.2 A/cm^2, which corresponded to the passage of a specific charge q=3.46·10^4 c/cm^2. After hydrogenation for 24 hours, the ε-phase was not detected. In our experiments, hydrogenation was carried out at a current density of 2 A/cm^2 for t=7 h, which corresponds to q=3.15·10^4 c/cm^2. It is clear that the values of q in [7] and in our experiments are close, which adds confidence to our argument about the decrease in electrical resistivity as a result of hydrogenation.

It should be noted that the decrease in electrical resistivity can occur due to discrete growth of crystallites of ε-hydride ZrH_{2-x}. This result follows from the core model of a two-phase material with inclusions of another phase in the nodes of the lattice in the form of series-connected cells with higher conductivity in a matrix with lower conductivity [20].

4. Conclusions

The XRD data show that as a result of electrolytic hydrogenation, a layer of δ-hydride $ZrH_{1.66}$ with a thickness of ≈9.5 μm is formed near the surface of wire samples of the Zr1Nb alloy. The layer consists of nanocrystallites that vary greatly in size for the (111) ($d_{(111)}$>100 nm) and (200) ($d_{(200)}$~6 nm) orientations along the normal to the wire surface due to its high crystallographic texture, which determines the least favorable direction for

hydrogen diffusion. Hydrogenation of the annealed samples leads to a decrease in the shear modulus by ≈10%, which indicates a lower mechanical stability of δ-hydride compared to α-Zr. The hydride phase formed in the deformed material is characterized by a weak change in the shear modulus, which indicates the competition of two factors: a decrease in the modulus due to the direct formation of the δ-phase and a recovery due to the relaxation of internal stresses.

The decrease in the electrical resistivity of the sample after hydrogenation is associated with a shunting effect due to the formation of a rather thin surface layer of ε-hydride with a higher conductivity compared to the δ-hydride layer and α-Zr matrix.

References

1. G.A.Nekrasova, Zirconium in the nuclear industry. Experience in operating cable pipes in CANDU reactors: Review, Vol. 14, Moscow: TsNIIatominform (1985).
2. P.A.Ponomarenko, E.P. Taborovskaya at al., *Nuclear and Radiation Safety*, 2(58), 36 (2013).
3. E.Y. Afanasieva, I. A. Evdakimov, O. V. Khoruzhii, V. V. Likhanskii, and A. A. Sorokin, *Trans. 17th Intern. Conf. on Structural Mechanics in Reactor Technology (SMiRT 17)*, Praque, Chech Repablic, August 17-22, 2003, Paper # C03-1.
4. Anna-Maria Alvarez Holston. In-pile and out-of pile methods to predict fuel cladding failures. SCIP Property Information. Studvik. October 2011.
5. R.M. Lobo, A.H.P. Andrade, and M. Castagnet, International Nuclear Atlantic Conference - INAC 2011, Belo Horizonte, MG, Brazil, October 24-28. 2011, Associacao Brasileira De Energia Nuclear - Aben. ISBN: 978-85-99141-04-5.
6. T.P. Chernyayeva, A.V. Ostapov, *Probl. Atomic Sci. Tech*., №5(87), 16 (2013).
7. Yu-Jie Jia, Irene J. Beyerlein, Wei-Zhong Han, *Acta Materialia*, **216**, 117146 (2021)
8. V.M. Azhazha, A.F. Bolkov, B.V. Borts, I.N. Butenko et al, *Probl. Atomic Sci. Tech*., №5, 110 (2005).
9. M.A.Krishtal, S.A.Golovin. Internal friction and structure of metals, Metallurgy, Moskow (1967).
10. D.G. Malykhin, K.V. Kovtun, T.S. Yurkova et. al. Surface purity effect on irregularity of changes in deformation texture of Zr-2.5%Nb alloy // East. Eur. J. Phys., **1**, 50 (2021).
11. L.I.Mirkin, Handbook on X-ray diffraction analysis of polycrystals, State ed. f.-m. literature, Moscow (1961).
12. R.M.Daum, Y.S.Chu, A.T.Motta, *J. Nucl. Mater*., **392**, No.3, 453 (2009).
13. W.J.Babyak, *Trans. AIME*, **239**, 232 (1967).
14. C.Roy, J.G.Jacques, *J. Nucl. Mater*., **31**, 233 (1969).
15. J.Huot. Hydrogen in Metalls. New Trends in Intercalation Compounds for Energy Storage, *NATO Science Series*, **61**, 109 (2002).
16. D.A.Papaconstantopoulos, B.M.Klein, E.N.Economou and L.L.Boyer, *Phys. Rev. B*, **17**, 141 (1978).
17. V.I.Sokolenko, A.O.Chupikov, M.M.Pylypenko, M.B.Lazareva, and O.Yu. Roskoshna, *Fizyka Nyzkykh Temperatur/Low Temperature Physics*, **50**, No. 2, 133 (2024).
18. P. Vajda, Handbook on the Physics and Chemistry of Rare Earths, North−Holland, Amsterdam, vol. 20 (1995).
19. P.W.Bickel, T.G.Berlincourt, *Phys. Rev. B*, **2**, 4807 (1970).
20. A.I. Kravchenko, *Probl. Atom. Sci. Technol,*. **20**, 41 (2014).